J. Phys.: Condens. Matter **22** (2010) 474001 (9pp) doi:10.1088/0953-8984/22/47/474001

Lateral uniformity in chemical composition along a buried reaction front in polymers using off-specular reflectivity*

Kristopher A Lavery[1,3], **Vivek M Prabhu**[1], **Sushil Satija**[2] **and Wen-li Wu**[1,4]

[1] Polymers Division, National Institute of Standards and Technology, Gaithersburg, MD 20899-8541, USA
[2] Center for Neutron Research, National Institute of Standards and Technology, Gaithersburg, MD 20899-8541, USA

E-mail: wenli@nist.gov

Received 25 September 2009, in final form 5 January 2010
Published 15 November 2010
Online at stacks.iop.org/JPhysCM/22/474001

Abstract
Off-specular neutron reflectometry was applied to characterize the form and amplitude of lateral compositional variations at a buried reaction–diffusion front. In this work, off-specular neutron measurements were first calibrated using off-specular x-ray reflectivity and atomic force microscopy via a roughened glass surface, both as a free surface and as a buried interface that was prepared by spin coating thin polymer films upon the glass surface. All three methods provided consistent roughness values despite the difference in their detection mechanism. Our neutron results demonstrated, for the first time, that the compositional heterogeneity at a buried reaction front can be measured; the model system used in this study mimics the deprotection reaction that occurs during the photolithographic process necessary for manufacturing integrated circuits.

1. Introduction

The ability to measure the structure of buried interfaces, directly and non-invasively, is highly desirable for research in many problems in physics, biology and materials science. The necessity for the observation of chemical or morphological processes occurring beneath a surface has driven the development of a number of measurement methods; unfortunately, most of these are destructive and require an etching or cleaving process to reveal the buried interfaces. Specular x-ray and neutron reflectometry have gained prominence in materials research due to their sensitivity to changes in interfacial roughness, film thickness, and effective refractive index [1]. As such, these techniques lend themselves to the study of polymer thin film confinement effects [2], phase behavior [3], polymer interdiffusion [4, 5], and reaction–diffusion processes [6].

While specular reflectometry provides nanometer structural resolution normal to the plane of the film, there is little information on the lateral structure. An aspect of interfacial characterization that suffers from this fact is the determination of the interfacial roughness. Deviations from the Fresnel specular reflectivity [1, 7] are attributed to interfacial widths as long as the lateral length scale of the roughness falls within the coherence length of the incident beam. Therefore, from specular reflection alone it is not possible to distinguish material gradients from physical roughness in the scattering length density. Separation of these two contributions is possible by measuring the in-plane component of the scattering by rocking about the specular condition in a transverse scan.

This paper describes the off-specular neutron reflectivity (OSNR) characterization of the roughness of a model buried interface; a roughened glass surface coated with a thin polystyrene film. Prior to being coated with polystyrene (PS), the glass surface was characterized with off-specular x-

* Official contribution of the National Institute of Standards and Technology; not subject to copyright in the United States.
[3] Present address: Qualcomm MEMS Technologies, Inc. 2581 Junction Avenue, San Jose, CA 95134, USA.
[4] Author to whom any correspondence should be addressed.

ray reflectivity (OSXR) and atomic force microscopy (AFM). The polystyrene overcoat on glass was introduced via spin coating and is not expected to change the glass roughness due to the inert solvents (non-etching) used. Deuterated polystyrene (dPS) was used to increase the contrast and facilitate the neutron measurements. Comparison of the roughness obtained from these complementary techniques verifies the interpretation of our results and supports the use of off-specular reflectivity for the characterization of buried interfaces. Next, a polymer bilayer designed to mimic an idealized photo-exposure, or a step function in initial acid concentration, is examined. Photogenerated acid molecules in the bottom polymer layer of the bilayer film stack diffuse and catalytically deprotect the acid-labile groups of the photoresist top layer. The shape of this buried reaction–diffusion front, in the form of compositional heterogeneities in both the lateral and longitudinal directions, is described using neutron off-specular reflectivity.

Advances in the theory of off-specular reflectivity [8–13] combined with the development of high-resolution, high-flux reflectometers [14] have enabled a wider use of this technique to explore interfacial problems. Recently, the use of grazing incidence small angle x-ray scattering (GISAXS) has garnered significant interest as a means of studying the lateral structure of thin films and surfaces using a 2D detection system and high-flux synchrotron x-ray sources. Unfortunately, research reactor neutron sources provide a flux many orders of magnitude lower than synchrotron x-ray sources, so that slit collimation is the only choice for OSNR. As a result, many of the recent advancements made in GISAXS are not applicable for this work because 2D GISAXS measurements take advantage of the pinhole collimation of the high intensity x-ray source. Desmearing off-specular data collected on a 2D detector from a slit-collimated neutron source is prohibitively difficult because the off-specular scattering is not isotropic. Therefore, transverse, or 'rocking' scans were used in this work.

2. Theory

This section describes the fundamentals for interpreting and analyzing the x-ray and neutron off-specular measurements. There is no difference in theoretical aspects between x-ray and neutron scattering except the calculation of scattering contrast. First there is a brief description of the Born approximation, followed by the distorted wave Born approximation (DWBA) proposed by Sinha for a rough surface of a single substrate [10]. Next, there is a discussion of an extension of the DWBA to the buried interfaces of multilayer structures. Only x-ray scattering will be mentioned in the following paragraph for illustration purposes, however, the discussion and general principles are equally valid for neutron scattering.

During recent years, grazing incidence x-ray techniques [15] have proven to be a powerful tool for assessing the near surface structure of numerous advanced materials. A typical experimental configuration for such measurements is illustrated in figure 1. A highly collimated beam of monochromatic x-rays impinges onto a flat specimen at a very

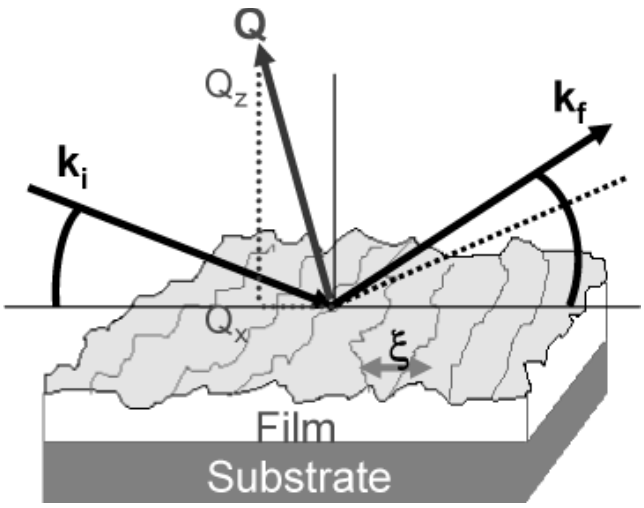

Figure 1. Experimental geometry for the reflectivity experiments in this work. k_i is the momentum of the incident beam and k_f is that of the reflected beam. Q_x and Q_z are the in-plane and perpendicular components of the scattering vector Q. ξ is the lateral correlation length.

small angle of incidence. Throughout this work the surface normal is denoted as the z-axis and the reflection surface is on the x–z plane. As the refractive index of all materials in the x-ray region is slightly less than unity, the beam is totally reflected if the incidence angle is smaller than some critical value, which is of the order of a fraction of a degree. Near the critical angle the penetration depth of the beam into the material is small, typically a few nanometers, and is the reason why grazing incidence x-ray techniques are inherently surface sensitive. When the incidence angle is increased far above the critical angle the penetration depth increases to a few micrometers and is determined by photoelectric absorption of the x-rays by the reflecting material.

The off-specular scattering amplitude $A(q)$ is typically modeled as

$$A(q) \propto \langle \psi_i | \rho(r) | \psi_s \rangle, \tag{1}$$

where ψ_i and ψ_s represent the incident and time reverse wavefunctions and are functions of the depth and the incident or scattering angles, i.e. they are $\psi_i(z, \theta_i)$ and $\psi_s(z, \theta_s)$. Here $\rho(r)$ is the scattering density function describing the interface topology as well as compositional fluctuations within the scattering material. Within the context of the Born approximation, the wavefunctions are assumed to be plane waves and are independent of the position r. The scattering intensity is simply $A(q)A^*(q)$, where $q = k_s - k_i$ is the scattering vector and k_i and k_s denote the incident and scattered wavevectors, respectively. When both the incident and the time reverse scattering wavefunctions are approximated as simple plane waves, equation (1) represents a Fourier transform of the scattering density function.

For off-specular scattering of a rough surface of a simple substrate, i.e., no compositional fluctuations within the material, Sinha [10] proposed that ψ_i remains as the incident plane beam wavefunction whereas ψ_s is replaced by the wavefunction of the transmitted component of the reflected

beam from an idealized reference surface with no roughness, i.e., Fresnel wavefunctions that consist of incident and partially reflected plane waves above the surface and a partially transmitted plane wave below the surface. Furthermore, the height or the position on the z-axis of the idealized or reference surface is chosen such that it coincides with the median plane of the rough surface. This is the so called distorted wave Born approximation (DWBA). It is worth noting that the calculated off-specular scattering intensity depends on the position of the idealized surface.

Often surface roughness and compositional fluctuations are simultaneously present at interfaces, making the position of the reference surface difficult to assign, especially for the cases with a multilayer. Wu [12] resolved this shortfall by proposing to replace a single reference surface with the laterally averaged interface profile denoted as $\langle\rho(z)\rangle$, to calculate both $\psi_{\rm i}(z,\theta_{\rm i})$ and $\psi_{\rm s}(z,\theta_{\rm s})$. In this approach there is no ambiguity in selecting the idealized surface to generate the wavefunctions used in the DWBA. In practice, the quantities $\langle\rho(z)\rangle$, ψ and $\psi_{\rm s}$ can all be readily generated via specular reflectivity measurements and modeling. $\langle\rho(z)\rangle$ is the scattering density profile deduced from specular reflectivity measurements, $\psi_{\rm i}$ and $\psi_{\rm s}$ are the by-products from the fitting process where the profile $\langle\rho(z)\rangle$ is represented by multilayer step functions. A similar approach was undertaken by Wormington *et al* [11], where the structure factor $\rho(r)$ was modeled as a multilayered structure and both compositional fluctuations and roughness are included explicitly at each interface. The calculation also includes correlations in roughness among different layers, important for multilayers. The wavefunctions $\psi_{\rm i}(r)$ and $\psi_{\rm s}(r)$ at each layer are calculated using a typical specular reflectivity fitting algorithm as proposed by Wu [12].

3. Experimental details[5]

3.1. Model substrates

Float glass substrates with 76.2 mm (3 in) diameter and 5 mm (0.197 in) nominal thickness, were used as the model substrates. The intrinsically smooth float glass surface served as one model surface, whereas a second sample was roughened using a sand etch at a glancing angle for 5 s that resulted in a slight frosting. This roughened wafer was cleaned with high pressure N_2 and soaked in acetone to remove any residual particulates. The surfaces were characterized by using tapping mode AFM and reflectivity methods before preparing the model buried interfaces.

3.2. Buried interface

The roughened substrate was subsequently coated with 100 nm of deuterated polystyrene (dPS) by spin coating from toluene. The sample was annealed at 160 °C for 24 h in order to relax the polymer, fill in the crevices on the substrate and remove any residual solvent. AFM measured the uniformity of the resulting dPS surface.

[5] Certain commercial equipment and materials are identified in this paper in order to specify adequately the experimental procedure. In no case does such identification imply recommendations by the National Institute of Standards and Technology nor does it imply that the material or equipment identified is necessarily the best available for this purpose.

3.3. Polymer–polymer bilayer

The bottom layer is a polymer loaded with photoacid generator (PAG) molecules. The top layer is the photoresist copolymer in which the protecting group was deuterated to provide neutron scattering length density contrast between protected and deprotected forms of the resist. The deprotection reaction for this photoresist is shown in figure 2(A). Bilayer thin films of poly(hydroxystyrene-*co*-d_9-tert-butyl acrylate) (PHOST-*co*-d_9-TBA) on poly(hydroxyladamantyl methacrylate) (PHAdMA) were prepared on smooth 76.2 mm (3 in.) diameter by 5 mm (0.197 in.) thick float glass substrates using subsequent spin coating steps (figure 2(B)). The PHAdMA bottom layer contained 6% by mass of triphenylsulfonium perfluorobutane sulfonate photoacid generator. Post-application bake steps were performed at 130 °C for 60 s to remove any residual solvent. The unexposed bilayer film was characterized using specular and off-specular neutron reflectivity. The same bilayer film was then exposed to 248 nm light for 10 s (Oriel Instruments), resulting in a dose of 2.6 mJ cm^{-2} and post-exposure baked (PEB) at 90 °C for 180 s. Specular and off-specular neutron reflectivity measurements were then completed identically to the unexposed bilayer.

3.4. Reflectivity

Figure 1 illustrates the experimental geometry. The dotted line represents the reflected beam at the specular condition, which places the scattering vector, Q, normal to the surface along Q_z. Rocking curves, or transverse scans, are performed by tilting the sample at a fixed detector angle, thus varying the incident angle, omega (ω), and keeping the scattering angle constant. This varies Q_x while keeping Q_z largely constant. Scanning away from the specular condition incorporates contributions from structures in the plane of the film, as illustrated by the solid lines, where $k_{\rm i}$ represents the incident x-ray beam and k_f represents the diffuse reflection.

Figure 3 shows the range of Q-space measured by these experiments. X-ray reflectivity measurements, shown in gray, were performed on a modified Scintag diffractometer using x-rays at a wavelength of 0.154 nm and slit collimation. The specular scan (dotted line) was taken over a Q_z range of (0.10 to 1.2) nm^{-1} with the sample substrate kept fixed and mounted horizontally. As mentioned above, off-specular transverse scans vary Q_x while keeping Q_z largely constant (dashed lines). These measurements were taken at three different Q_z values, (0.21, 0.55, and 0.99) nm^{-1}, and scanned over the complete angular range. The angular range is defined by the plane of the substrate, and the resulting experimental limits in Q-space are illustrated by the solid curves.

Neutron reflectivity experiments, shown in black in figure 3, were performed on the advanced neutron diffractometer/reflectometer (AND/R) beam line at the NIST Center for Neutron Research. A neutron wavelength of 0.500 nm with slit collimation was used for these measurements. Specular scans (dotted line) were taken over a Q_z range of (0.10 to 0.90) nm^{-1} with the substrate mounted vertically. The resolution of this instrument was determined to be 0.018 in terms of $\Delta Q/Q$. A constant value of resolution was achieved by increasing the slit

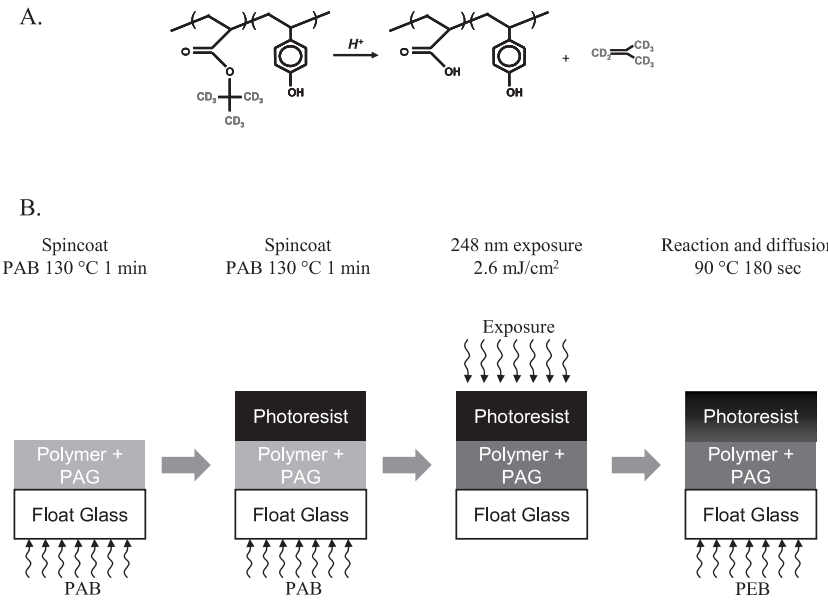

Figure 2. (A) The deprotection chemistry of poly(hydroxystyrene-*co*-d_9-tert-butyl acrylate) (PHOST-*co*-d_9-TBA) and (B) the processing steps used to fabricate the polymer/polymer bilayer and create the reaction/diffusion front.

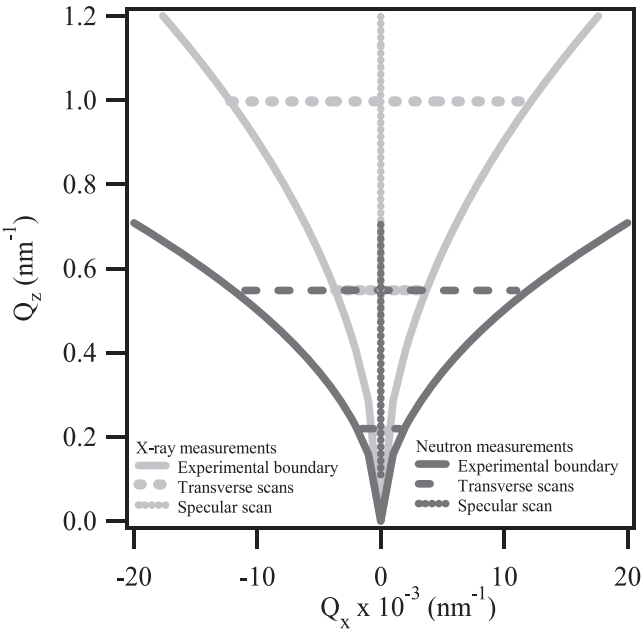

Figure 3. The Q_x and Q_z space explored in this work. Regions below the solid curves are not accessible experimentally.

opening with Q. Transverse scans (dashed lines) were taken at two Q_z values, (0.22 and 0.55) nm^{-1}, chosen to coincide with the range used in the x-ray measurements. The incident beam and detector slits were set to be equal and constant over the full rocking range, being 0.4 mm at $Q_z = 0.22\ nm^{-1}$ and 1 mm at $Q_z = 0.55\ nm^{-1}$. The lateral coherence length at the measurement condition set the upper limit of the detection limit of the lateral length of the interface roughness, its value can be estimated as $\lambda/\Delta\theta \sin\theta_i$ for a reflection condition from a flat surface [23]. $\Delta\theta$ is the angular divergence of the source seen by the sample and θ_i is the incident angle. Based on the above relation the lower bound of the lateral coherence length is 5 μm and 31 μm for off-specular scans at $Q_z = 0.22\ nm^{-1}$ and $0.55\ nm^{-1}$ respectively. For all the x-ray off-specular scans the lower bound of the lateral coherence length was estimated at 12 μm.

All of the specular neutron and x-ray reflectivity data in this work were fitted using a Parratt formalism [16]. A Levenberg–Marquardt nonlinear least-squares fitting routine [17] aided in finding the best fit values that provide a meaningful analysis and design of the off-specular experiments. Uncertainties in the fit parameters were calculated as an estimated standard deviation from the mean. Where the standard deviation limits are smaller than the plot symbols the brackets were left off for clarity. The off-specular data analysis was conducted using the computer code developed by Wormington [13], utilizing a genetic algorithm routine to generate best fits to the data. As proposed in the work by Wu [12], this algorithm applied the numerical results obtained by fitting the specular data via Parratt formalism as the wavefunction along the z-axis at each layer, i.e. at the final convergent condition in the fitting of specular data the resultant wavefunctions were reserved and used as the ψ_i and ψ_s along the z-axis. This approach is different from many others using an analytic equation to approximate ψ_i and ψ_s. The in-plane component of both ψ_i and ψ_s in equation (1) stays unperturbed, as for the case of the Born approximation. In our approach equation (1) will result in off-specular intensities only when some in-plane component exists in $\rho(r)$, otherwise equation (1) will result in specular intensities only and its value is consistent with the experimental values. In this approach the existence of multiple interfaces, e.g. air/dPS free surface and dPS/glass interface in one of the sample configurations, is encompassed.

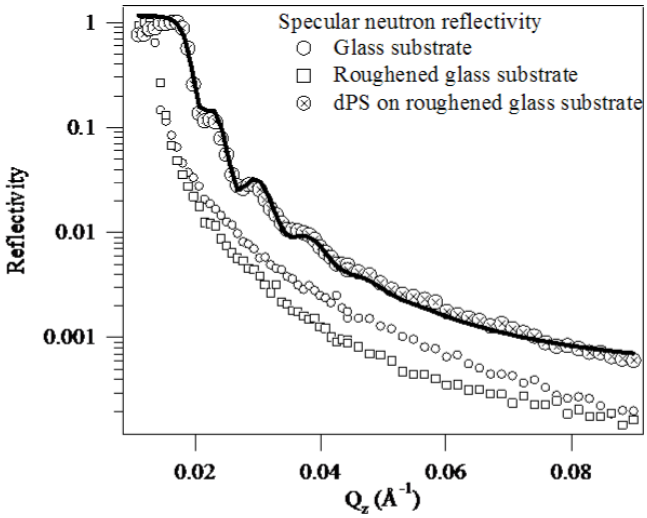

Figure 4. Specular neutron reflectivity measurements on bare float glass, roughened float glass (shifted down by 2 decades) and dPS-coated rough float glass (shifted down by 3 decades). Solid lines are fits to the data.

4. Results and discussion

4.1. Specular reflectivity

The smooth and roughened float glass substrates were characterized by specular neutron reflectivity, as shown in figure 4. The smooth substrate had a surface rms (root mean square) roughness of (0.6 ± 0.3) nm as characterized by AFM, which was comparable to that obtained by neutron reflectivity. The roughened float glass, shown with a different symbol, had a surface roughness of (4.9 ± 0.6) nm, found using both specular XR and NR. The rms analysis of the AFM data reveals a roughness of (4.5 ± 0.6) nm that is comparable within the uncertainty of the measurement. It is evident that a rapid decay of the neutron reflectivity intensities occurred after the critical angle for the roughened glass, however, the intensity levels off at high Q. This is presumably due to strong diffuse scattering of the roughened surface.

The reflectivity from the deuterated polystyrene coated rough glass is distinguished from the bare substrate by the presence of Kiessig fringes. Additionally, the rapid decay in Kiessig fringe amplitude with increasing Q_z is indicative of the rough buried interface, and the higher critical angle of reflection is due to the higher scattering length density of the dPS in comparison to float glass. Upon model fitting, the buried interfacial width between the glass and polymer did not change due to the uniform coating of the roughened glass. The air/polymer surface interfacial width was 1 nm.

4.2. Off-specular reflectivity: model float glass interface

A representative x-ray transverse scan curve is shown in figure 5. Specular reflectivity experiments give important initial information for analysis of off-specular data. The real and imaginary components of the refractive index were determined from the critical angle for the bare substrate and the dPS-coated wafer. Additionally, the interfacial roughness gives important information regarding the interfacial width. A modified form of the distorted wave Born approximation model was used to fit the data. Following Sinha [10], the surface topology is described by the height–height correlation function $\langle \eta(0)\eta(X)\rangle$,

$$C(X) = \langle \eta(0)\eta(X)\rangle = \sigma_{\mathrm{R}}^2 \exp -\left|\frac{X}{\xi}\right|^{2H}, \qquad (2)$$

where the quantity $\eta(X)$ denotes the center of the interfacial profile, X is the separation between two points, and the $\langle \cdots \rangle$ represents a configurational average. The topology in this instance is described by a self-affine fractal surface [18]. The lateral correlation length, ξ, is described as the fractal cut off length, and the surface fractal dimension is described by the Hurst parameter, H, where the fractal dimension $d = 3 - H$. Previous work [11, 19, 20] has shown that the surfaces of glass substrates display an H value of $\approx$0.3, and this value was kept constant in the analyses that follow. In the case of comparing OSXR results from roughened bare glass surface with OSNR results from buried glass surface, keeping H at 0.3 merely simplified the data analysis and did not imply this H value was an optimal one. For the case of OSNR measurement of compositional heterogeneity along a buried reaction front, fixing H at 0.3 seems to fit the data well and no effort was spent to identify the optimal value for H, primarily due to the limited amount of OSNR data available in this work. An extensive OSNR data set covering a broad Q range will be needed to identify the best fit of H.

In addition to fitting the lateral length scale, ξ, off-specular reflectivity offers the unique advantage of being able to distinguish between the roughness of a sharp interface characterized as an amplitude, σ_{R}, and a gradient at the interface, σ_{G}. The gradient is in the scattering contrast across the interface. The two different modes of contrast, electron density for x-rays and neutron scattering length density for neutrons, makes x-rays and neutrons sensitive to different aspects. In the present case we use the enhanced contrast provided by deuterium labeled polystyrene to probe the buried interface with higher sensitivity and contrast than the electron density difference from x-ray reflectivity.

The difference in diffuse scattering for physical roughness and gradient is illustrated in figure 5. If the scattering length density, averaged within the footprint of the beam, changes equally as a function of depth there will be no difference in the specular reflectivity from the three cases shown. This condition is confirmed by the constant intensity of the specular peak, i.e., they will give the same values for the interfacial width, σ. The surface roughness obtained from specular reflectivity on this surface would have contributions from both gradient and roughness such that

$$\sigma_{\mathrm{spec}}^2 = \sigma_{\mathrm{R}}^2 + \sigma_{\mathrm{G}}^2. \qquad (3)$$

The interfacial width σ_{spec} determined by specular reflectivity provides a constraint for the off-specular data fits in order to satisfy equation (3). The above equation implies the local gradient and local roughness are uncorrelated. This is consistent with the model of compositional heterogeneity

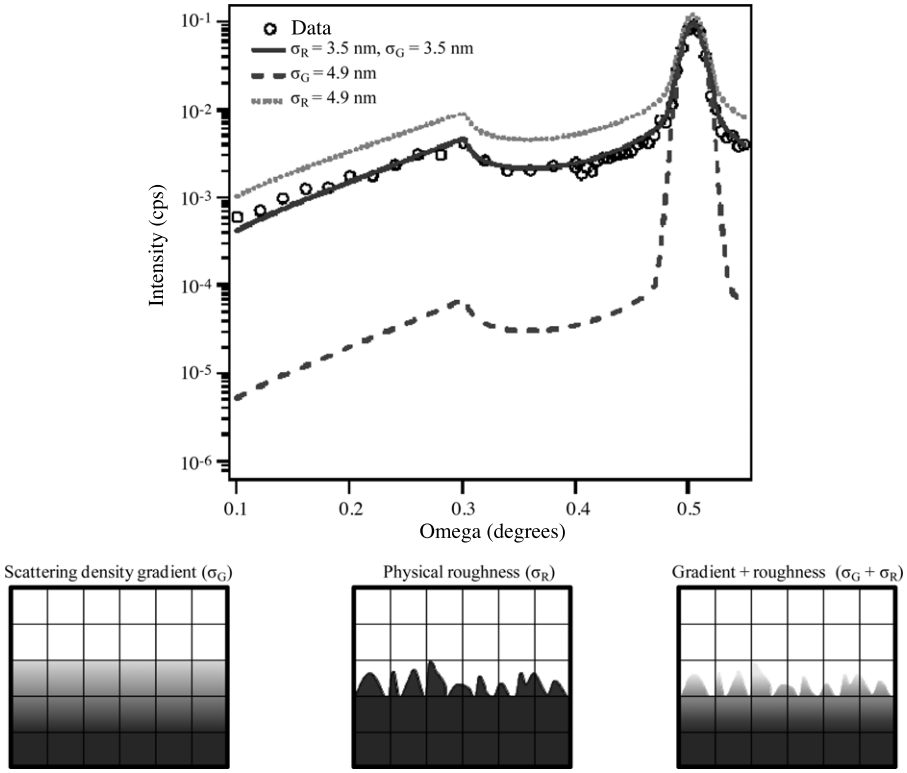

Figure 5. Fit to the off-specular neutron reflectivity data near $Q_z = 0.22\ \text{nm}^{-1}$ combining physical roughness with a chemical gradient for the dPS/roughened float glass sample. For comparison the calculated curves for an interface having only a chemical gradient (σ_G) and only a physical roughness (σ_R) are included.

along a latent reaction front used in the present study; our model, illustrated in figure 5, calls for a uniform compositional gradient along the direction of the average reaction propagation while it allows the front to stay non-planar or rough. Figure 5 shows off-specular neutron reflectivity data that illustrates the impact of the relative contribution of σ_G and σ_R for the rough glass substrate underneath a layer of dPS. From the specular measurement σ_{spec} is found to be (4.9 ± 0.6) nm. When all of the roughness is placed into the gradient term (dashed curve) there is a lower intensity for the diffuse scattering, while the specular intensity does not change. This is because there is no diffuse scatter from the glass surface; only an average scattering length density gradient across the interface. If all of the roughness is placed into the σ_R term (dotted line) the diffuse scattering intensity increases due to the physical roughness of the interface. A combination of the two contributions is required to obtain the best fit (solid curve) while satisfying equation (3).

The data in figure 6 show x-ray off-specular reflectivity curves at three different Q_z values, (0.22, 0.55 and 0.99 nm^{-1}). Performing measurements at multiple angles provides several advantages in improving the reliability of the fitting process. The fit parameters for ξ, σ_G, and σ_R had to fit at all three angles. In addition, each scan range exhibits sensitivity to a different range of lateral length scales. The low Q_z transverse scan at 0.22 nm^{-1} was sensitive to length scales on the order of microns, while the intermediate Q_z scan was sensitive to $\approx$100 nm, and the high Q_z scan was sensitive to ξ values on the order of $\approx$10 nm (see figure 3). Fits to the data illustrate a significant change in the form of the surface roughness before and after roughening. σ_R increases from 0.6 to 3.5 nm, σ_G increases from 0 to 3.5 nm, while the correlation length, ξ, decreases from (1500 ± 150) nm to (500 ± 100) nm.

It is useful to compare the correlation length obtained from scattering to that obtained using power spectral density analysis of AFM data. These data for the roughened float glass are summarized in table 1. The smooth float glass sample, which had a rms roughness of (0.6 ± 0.3) nm, displayed a maximum in power spectral density at (1800 ± 100) nm. This is on the order of the correlation length obtained using OSXR. It is noteworthy that the roughness, σ_R, of the roughened glass surface is 3.5 ± 0.3 for OSXR and 4.5 ± 0.6 for AFM. This slight difference in the two values may be due to the statistical nature of the scattering experiment in averaging over a larger portion of the surface than the AFM measurement over a few orders of magnitude; of the order of cm^2 versus μm^2. Even so, despite the differing nature of the two measurements, the dominant lateral length scales obtained were in good agreement. This was also the case with the roughened surface. AFM revealed a maximum in power spectral density at (600 ± 100) nm, compared to the ξ of (500 ± 100) nm obtained by OSXR.

Once the bare surface was fully characterized, off-specular neutron reflectivity was used to measure the buried interfacial roughness between the rough float glass substrate and the dPS top layer. Measurements were performed at two Q_z values, 0.22 nm^{-1} and 0.55 nm^{-1}, that are sensitive to lateral length scales on the order of micrometers and $\approx$100 nm, respectively,

Table 1. Roughness parameters for the roughened float glass substrate. Off-specular x-ray (labeled as x-ray) and AFM data are from the bare substrate. Off-specular neutron data (labeled as neutron) are from the dPS/rough glass interface.

	σ_R (nm)	σ_G (nm)	ξ (nm)	H	$\sqrt{\sigma_R^2 + \sigma_G^2} = \sigma_{spec}$ (nm)
X-ray	3.5 ± 0.3	3.5 ± 0.3	500 ± 100	0.3	4.9 ± 0.6
AFM	4.5 ± 0.6	N/A	600 ± 100	N/A	4.5 ± 0.6
Neutron	3.5 ± 0.3	3.5 ± 0.3	500 ± 100	0.3	4.9 ± 0.6

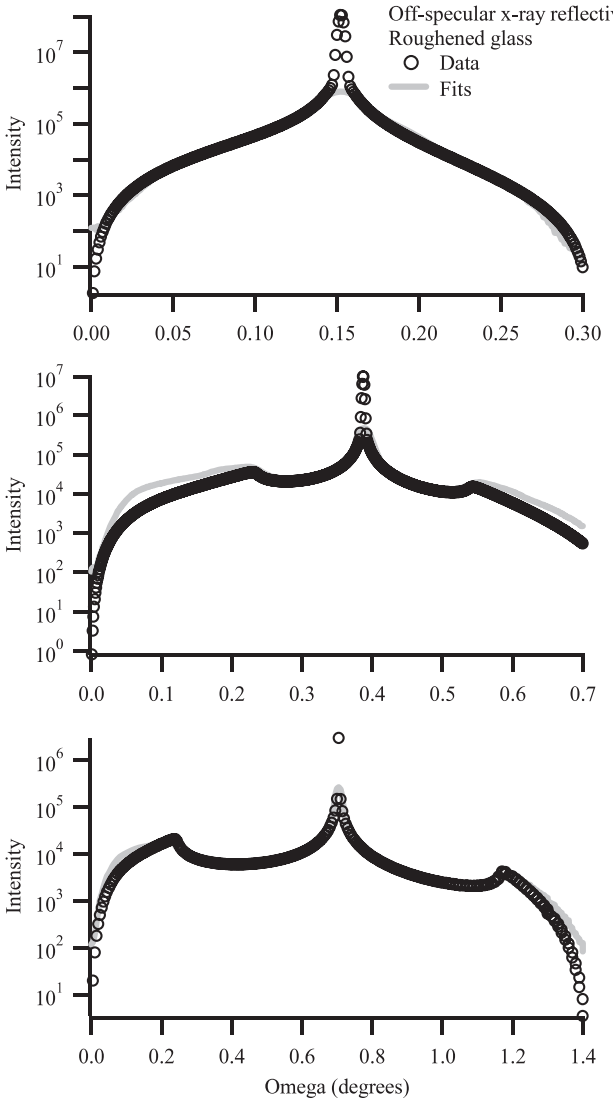

Figure 6. Off-specular x-ray reflectivity data and fits of bare roughened glass at Q_z of 0.22 nm^{-1} (top), 0.54 nm^{-1} (middle), and 0.99 nm^{-1} (bottom).

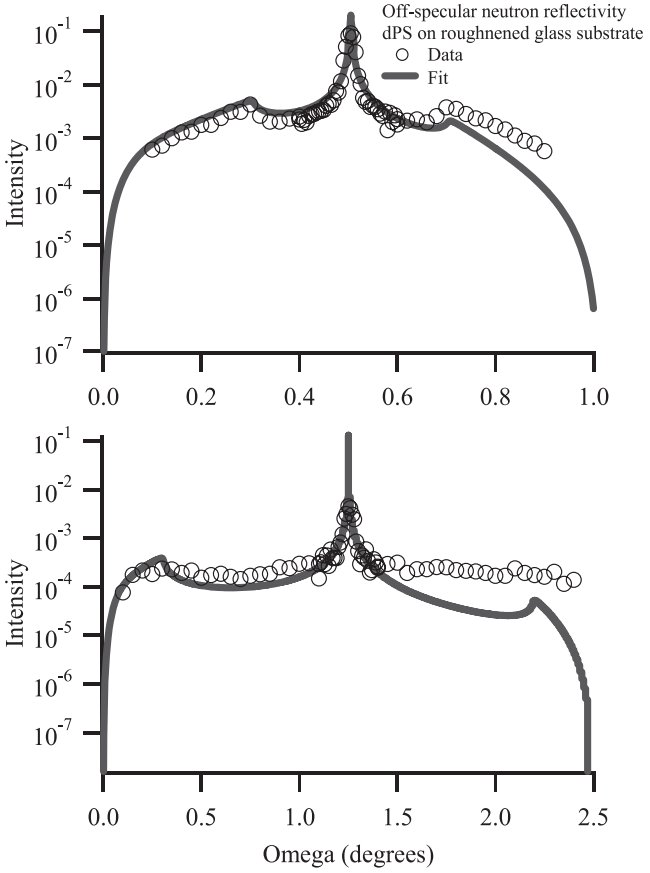

Figure 7. Off-specular neutron reflectivity data from dPS covered roughened glass surface and fits at Q_z of 0.22 nm^{-1} (top) and 0.55 nm^{-1} (bottom).

as per figure 3. The low intensity of the off-specular scattering at larger Q_z values made analysis of the diffuse scattering inconclusive. Figure 7 shows fits to the data at these two angles. The best fit of the roughness parameters are shown in figure 5 with σ_G and σ_R equal to (3.5 ± 0.3) nm for $\xi = (600 \pm 100)$ nm. These values, within experimental error, are equivalent to those obtained using x-rays on the bare substrate. The existence of a gradient contribution in the roughened sample is evidence for roughness on a sub-100 nm length scale, which is not resolved at the Q_x range we measured. However, roughness on this length scale still contributes to the broadening of the interface, and the diffuse contribution becomes incorporated into the σ_G term. Keeping this caveat in mind, the compatibility of OSXR and OSNR, with differing mechanisms of scattering contrast, highlights the reliability and versatility of these measurements. It is worth noting that all the deduced lateral correlation lengths from OSXR and OSNR are less than the instrument lateral coherence length at the measurement settings specified previously.

We measured the lateral heterogeneity of a mechanically roughened glass surface both as a free surface and as a buried interface. No compositional or density gradient is expected to exist along the surface normal, i.e., σ_G equal to zero. However, the neutron and x-ray results can only be fitted with a gradient in composition across the buried interface. Moisture absorption near the glass/dPS interfaces maybe the culprit of this apparent gradient.

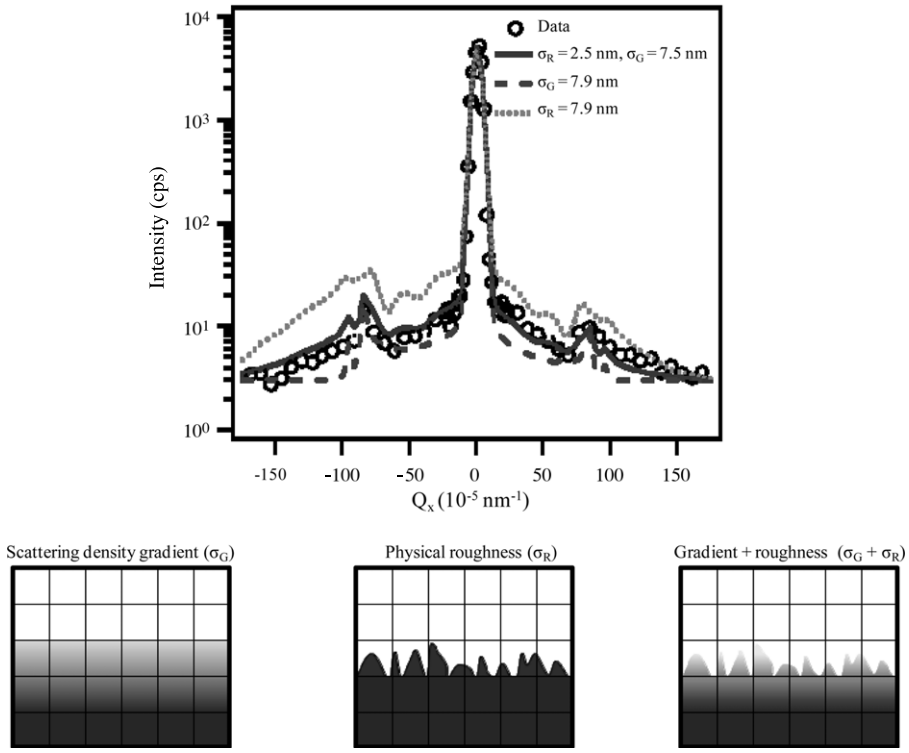

Figure 8. Fit to the off-specular neutron reflectivity data combining physical roughness with a chemical gradient for the reacted photoresist/polymer bilayer. For comparison the calculated curves for an interface having only a chemical gradient (σ_G) and only a physical roughness (σ_R) are included.

4.3. Off-specular reflectivity: photoresist reaction–diffusion front

The methodology described above was then applied to the photoresist polymer–polymer bilayer system described earlier [21, 22]. During the post-exposure bake (PEB), the activated photoacids in the bottom layer diffuse into the photoresist layer, catalyzing deprotection reactions. The *t*-butyl protecting groups are deuterium labeled, allowing one to follow the deprotection reaction–diffusion front propagation using neutron reflectometry [21]. Specular neutron reflectometry measurements were first performed to find the spatial extent of the reaction–diffusion front. The reaction–diffusion front width, σ_{spec}, was found to be 7.9 nm, calculated from the measured interfacial width of the reacted sample minus the initial bilayer interfacial width. In order to differentiate between interfacial width and roughness, the fitting parameters were systematically changed to obtain the most reliable fit to the data. Figure 8 shows calculations of the diffuse scattering compared to data taken after PEB at a Q_z of 0.22 nm^{-1}. If the interfacial width is modeled purely by lateral compositional variation, the result (dotted curve) overestimates the diffuse scattering intensity. On the other hand, if the reaction front is modeled as a smooth gradient in reaction extent without any lateral compositional inhomogeneity, the result (dashed curve) underestimates the diffuse scattering. The best fit was obtained by a combination of these contributions, where a lateral compositional inhomogeneity was added at the leading edge of the reaction front, while the region with a high degree of reaction stays laterally smooth. The result, shown as the solid curve in figure 8, is calculated with a combination of a smooth 7.5 nm compositional gradient and a 2.5 nm amplitude roughness superimposed at the leading edge of the reaction front. In all cases, H was kept fixed at 0.3.

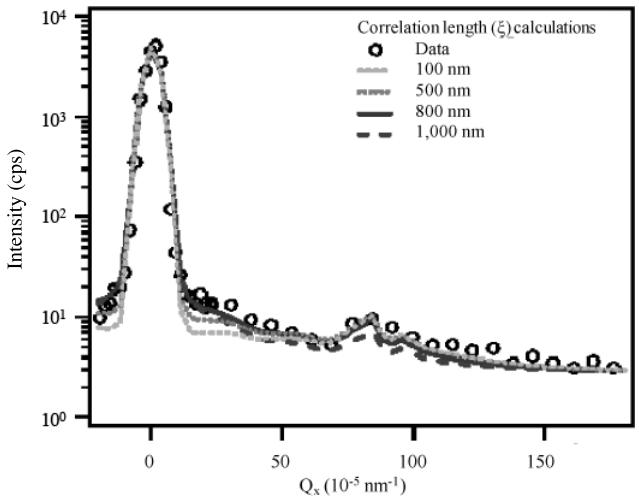

Figure 9. Fits to the bilayer off-specular neutron reflectivity data, systematically varying the correlation length used in the fit.

The lateral length scale of the compositional heterogeneity is determined through fits to the experimental results, using theoretical curves calculated with different values of ξ, as shown in figure 9. At a ξ of 800 nm the calculated result fits well with the diffuse scattering around the specular

peak and with the intensity of the Yoneda peak. Before reaction, the value of ξ is 1500 nm. A lateral correlation length of 800 nm is considered to be very relevant in semiconductor applications where the typical length scale of long-wavelength roughness along reaction front is near 500 nm. Off-specular reflectivity provides a complete picture of the buried deprotection reaction–diffusion front in a model photoresist copolymer for lithography with extreme-ultraviolet light. These measurements show the latent image possesses a low-amplitude, low-frequency inhomogeneity or roughness at the tip of the reaction wavefront.

5. Conclusions

Off-specular reflectivity was used to characterize the lateral length scale and the amplitude of the roughness at a buried interface. The bare surface roughness characterized by AFM and OSXR were consistent with the buried interface case using OSNR. The ability to separate physical roughness from a gradient interface was complicated by the presence of sub-100 nm lateral length scales that can contribute to the gradient term. OSNR was further applied to a more complicated buried reaction–diffusion problem, giving unprecedented detail to the structure of the buried chemical variation in the reaction front wave. These results illustrate the utility of off-specular measurements for a wide variety of buried interface problems.

Acknowledgments

This work was supported by a cooperative research and development agreement (CRADA) between Intel Corporation and NIST, CRADA 1893 as well as the NIST Office of Microelectronics Programs. KAL was supported by the NIST-NRC Postdoctoral Associateship Program. The authors acknowledge Kwang-Woo Choi and George Thompson at Intel Corporation and Saibal Basu at the NIST Center for Neutron Research for their helpful discussions and insights.

References

[1] Russell T P 1990 *Mater. Sci. Rep.* **5** 171
[2] Lambooy P *et al* 1994 *Phys. Rev. Lett.* **72** 2899
[3] Anastasiadis S H, Russell T P, Satija S K and Majkrzak C F 1989 *Phys. Rev. Lett.* **62** 1852
[4] Karim A, Felcher G P and Russell T P 1994 *Macromolecules* **27** 6973
[5] Gupta R R *et al* 2003 *Macromolecules* **36** 346
[6] Lin E K *et al* 2002 *Science* **297** 372
[7] Born M and Wolf E 1999 *Principles of Optics* (Cambridge: Cambridge University Press)
[8] Holy V and Baumbach T 1994 *Phys. Rev.* B **49** 10668
[9] Pynn R 1992 *Phys. Rev.* B **45** 602
[10] Sinha S K, Sirota E B, Garoff S and Stanley H B 1988 *Phys. Rev.* B **38** 2297
[11] Wormington M *et al* 1996 *Phil. Mag. Lett.* **74** 211
[12] Wu W L 1993 *J. Chem. Phys.* **98** 1687
[13] Wormington M, Panaccione C, Matney K M and Bowen D K 1999 *Phil. Trans. R. Soc.* A **357** 2827
[14] Dura J A *et al* 2006 *Rev. Sci. Instrum.* **77** 074301
[15] Bowen D K and Wormington M 1993 *Adv. X-ray Anal.* **36** 171
[16] Parratt L G 1954 *Phys. Rev.* **95** 359
[17] Press W 1986 *Numerical Recipes: The Art of Scientific Computing* (Cambridge: Cambridge University Press)
[18] Mandelbrot B B 1983 *The Fractal Geometry of Nature* (San Fransisco, CA: Freeman)
[19] Pape I, Hase T P A, Tanner B K and Wormington M 1998 *Physica* B **253** 278
[20] Pape I, Tanner B K and Wormington M 1999 *J. Non-Cryst. Solids* **248** 75
[21] Lavery K A *et al* 2006 *J. Vac. Sci. Technol.* B **24** 3044
[22] Lavery K A *et al* 2008 *Appl. Phys. Lett.* **92** 064106
[23] Salditt T, Rhan H, Metzger T H, Peosl J, Schuster R and Kotthaus J P 1994 *Z. Phys.* B **96** 227